Atmos. Chem. Phys. Discuss., 15, 10163–10198, 2015
www.atmos-chem-phys-discuss.net/15/10163/2015/
doi:10.5194/acpd-15-10163-2015


Atmospheric Chemistry and Physics
Discussions
Open Access



# Detection of anthropogenic dust using CALIPSO lidar measurements

**J. Huang[1], J. Liu[1], B. Chen[1], and S. L. Nasiri[2]**

[1]Key Laboratory for Semi-Arid Climate Change of the Ministry of Education, College of Atmospheric Sciences, Lanzhou University, Lanzhou, 730000, China
[2]Department of Atmospheric Science, Texas A&M University, College Station, TX, USA

Received: 5 March 2015 – Accepted: 10 March 2015 – Published: 7 April 2015

Correspondence to: J. Huang (hjp@lzu.edu.cn)

Published by Copernicus Publications on behalf of the European Geosciences Union.

## Abstract

Anthropogenic dusts are those produced by human activities on disturbed soils, which are mainly cropland, pasture, and urbanized regions and are a subset of the total dust load which includes natural sources from desert regions. Our knowledge of anthropogenic dusts is still very limited due to a lack of data on source distribution and magnitude, and on their effect on radiative forcing which may be comparable to other anthropogenic aerosols. To understand the contribution of anthropogenic dust to the total global dust load and its effect on radiative transfer and climate, it is important to identify them from total dust. In this study, a new technique for distinguishing anthropogenic dust from natural dust is proposed by using Cloud-Aerosol Lidar and Infrared Pathfinder Satellite Observation (CALIPSO) dust and planetary boundary layer (PBL) height retrievals along with a land use dataset. Using this technique, the global distribution of dust is analyzed and the relative contribution of anthropogenic and natural dust sources to regional and global emissions are estimated. Results reveal that local anthropogenic dust aerosol due to human activity, such as agriculture, industrial activity, transportation, and overgrazing, accounts for about 25 % of the global continental dust load. Of these anthropogenic dust aerosols, more than 53 % come from semi-arid and semi-wet regions. Annual mean anthropogenic dust column burden (DCB) values range from 0.42 $\mathrm{g\,m^{-2}}$ with a maximum in India to 0.12 $\mathrm{g\,m^{-2}}$ with a minimum in North America. A better understanding of anthropogenic dust emission will enable us to focus on human activities in these critical regions and with such knowledge we will be better able to improve global dust models and to explore the effects of anthropogenic emission on radiative forcing, climate change and air quality in the future.

## 1 Introduction

Dust accounts for some of the highest atmosphere mass loadings in the atmosphere and plays an important role in modulating radiative forcing and climate via a number of complex processes. While mineral dust has a wide distribution and relatively large optical depths, the existing atmospheric dust load cannot be explained by natural sources alone (Tegen and Fung, 1995). The atmosphere dust load that originates from disturbed soils by human activities, which can be interpreted as “anthropogenic” dust (Tegen and Fung, 1995), such as land use practices, can increase dust loading which, in turn, affects the radiative forcing. It is critical to quantify the relative importance of the different types of dust sources and the factors that affect emissions to understand the global dust cycle and historical and possible future changes in dust emissions, as noted by Okin et al. (2011) and Bullard et al. (2011).

Generally, anthropogenic dust originates mainly from agricultural practices (harvesting, ploughing, overgrazing), changes in surface water (e.g., shrinking of the Caspian and Aral Sea, Owens Lake), and also from urban practices (e.g., construction), and industrial practices (e.g., cement production, transport) (Prospero et al., 2002). Over the last few decades, a combination of more frequent warmer and dryer, winters and springs in semi-arid and semi-wet regions and changes in vegetated land cover due to human activity have likely increased anthropogenic dust emissions (Mahowald and Luo, 2003; Moulin and Chiapello, 2004; Tegen et al., 2004). Mulitza et al. (2010) demonstrated that the development of agriculture in the Sahel corresponded to a very large increase of dust emission and deposition in the region. The current consensus is that up to half of the modern atmospheric dust load originates from anthropogenically-disturbed soils (Tegen et al., 2004). In additional, Sokolik and Toon (1996) revealed that the direct solar radiative forcing by anthropogenic dust has a wide range of uncertainty and the forcing by anthropogenically-generated dust aerosols may be comparable to the forcing by other anthropogenic aerosols. Therefore, a clear understanding of anthropogenic dust emission is critical for predicting how changes in land usage (and thus changes in land use policies) will influence dust emission, loading, and deposition in the future (Okin et al., 2011).

However, the assessment of the role of anthropogenic activity in the atmospheric dust cycle is limited by the accuracy of the available data sets (Mahowald et al., 2002).





ACPD
15, 10163–10198, 2015

There are large uncertainties regarding the impact of anthropogenic activities on modulating dust emission directly (Sokolik and Toon, 1996) and understanding of the radiative forcing due to dust e.g., by disturbing soils, removing vegetation cover, or desiccating water bodies, and indirectly, by changing climate and the hydrological cycle requires an improved data set. Although there are many examples of humans altering their environment and thereby causing an additional dust burden, it is a challenging problem to separately quantify both the natural and anthropogenic components of the mineral aerosol (Sagan et al., 1979). Sokolik and Toon (1996) roughly assumed that the dust production rate is linearly proportional to the dust source area and estimated the amount of anthropogenic mineral aerosols through assessments of the land area converted to deserts by human activities. Tegen and Fung (1995) estimated the anthropogenic contribution to mineral dust to be 30 to 50 % of the total dust burden in the atmosphere by a three-dimension atmospheric dust transport model. Later, Tegen et al. (2004) provided an updated estimate by comparing observations of visibility and suggested that only 5 to 7 % of mineral dust comes from anthropogenic sources by calibrating a dust-source model with emission indices derived from dust-storm observations. Understanding of the emissions of anthropogenic dust is still very limited due to the difficulty of identifying and measuring them, which derives from the strong heterogeneities in the sources (Mahowald et al., 2002). Ginoux et al. (2012) was one of the first studies to estimate anthropogenic dust emissions using observations. They estimated that 25 % of dust is anthropogenic by using observation data, the Moderate Resolution Imaging Spectroradiometer (MODIS) Deep Blue satellite products, in combination with a land-use fraction dataset. A limitation of these products is that they can only be retrieved over bright surfaces in the visible wavelengths, excluding forests and ocean surfaces. Additionally, MODIS products do not include information about vertical distribution and therefore cannot readily exclude natural dust aerosol from deserts or marine seasalt aerosol that are transported over anthropogenic sources.

The Cloud-Aerosol Lidar and Infrared Pathfinder Satellite Observations (CALIPSO) satellite carries a lidar to actively remotely sense cloud and aerosol vertical profiles

(Winker et al., 2007; Hu et al., 2007a, b, 2009). CALIPSO can provide new insight into the detection of global anthropogenic dust emission due to its measurement of vertical resolution and polarization ratio. In this study, we develop a new technique for detection of anthropogenic dust emissions by using CALIPSO lidar measurements and use this to analyze its global distribution. Section 2 presents the data used in this study, while the method for separating anthropogenic dust from natural dust is outlined in Sect. 3. Section 4 discusses the calculation of anthropogenic dust column burden. Section 5 presents the global distribution of anthropogenic dust. Finally, the conclusions are presented in Sect. 6.

## 2 Data

### 2.1 CALIPSO data

This study relies on the CALIPSO Cloud-Aerosol Lidar with Orthogonal Polarization (CALIOP) for dust detection. CALIOP acquires vertical profiles of elastic backscatter at two wavelengths (532 and 1064 nm) and linear depolarization at 532 nm from a near nadir-viewing geometry during both day and night (Winker et al., 2007; Hu et al., 2007a, b, 2009). This study uses Level 1 backscatter, depolarization ratio, and color ratio profiles along with the Level 2 Vertical Feature Mask (VFM) products and 5 km Aerosol Profile Products. The depolarization ratio is a useful indicator for identifying non-spherical particles, and it can distinguish between atmospheric dust and spherical aerosols (Liu et al., 2004). The CALIPSO algorithm classifies aerosol layers that have volume depolarization ratio ($\delta_v$) greater than 0.075 as dust (Omar et al., 2009; Mielonen et al., 2009). Mielonen et al. (2009) also confirmed that classification of dust is more reliable than classification of fine aerosols because depolarization ratio can be used to distinguish non-spherical aerosols from spherical ones while the color ratio is sensitive mainly to particle size.





ACPD
15, 10163–10198, 2015

The CALIPSO Level 2 lidar VFM product (Liu et al., 2004; Vaughan et al., 2004) provides information about cloud and aerosol layer boundaries and positions. In CALIPSO Version 3 VFM data, the cloud aerosol discrimination (CAD) algorithm separates clouds and aerosols based on multi-dimensional histograms of scattering properties (e.g., intensity and spectral dependence), that is, the altitude-and latitude-dependent feature integrated color ratio, $\chi'$, the layer-integrated volume depolarization ratio, $\delta_v$, and the feature mean attenuated backscatter coefficient, $\beta'_{532}$ (Liu et al., 2010). The CAD score reflects their confidence that the feature under consideration is either an aerosol or a cloud, on a scale from −101 to 105. The larger the magnitude of the CAD score, the higher our confidence that the classification is correct. Liu et al. (2010) revealed that the confidence in the classification is high with $|CAD| \geq 70$ in Version 3. Based on this, we only include features with absolute values of CAD score greater than 70 in this study.

The Level 2 Aerosol Profile Product (Young and Vaughan, 2009) provides profiles of particle extinction coefficient and backscatter and additional profile information. In addition, the CALIPSO extinction quality control (QC) flags were also provided. Extinction QC = 0 (the lidar ratio is unchanged during the extinction retrieval) and QC = 1 (if the retrieval is constrained) are chosen in this paper, which are used to calculate optical depth by integrating extinction coefficients. Chen et al. (2013) noted that the impact of the screening procedure in this specific case is negligible.

## 2.2 Land cover data

The Collection 5.1 MODIS global land cover type product (MCD12C1) from 2011 is used in this study to provide anthropogenic dust source types. The MCD12C1 product has 0.05° spatial resolution, includes 17 different surface vegetation types, and was developed by the International Geosphere-Biosphere Programme data (IGBP) (Loveland and Belward, 1997; Friedl et al., 2010). It provides the dominant land cover type as well as the sub-grid frequency distribution of land cover classes within each 0.05° cell. Because we are focusing on sources of anthropogenic dust in this paper, we limit





ACPD
15, 10163–10198, 2015

our study to three agricultural surface types: Croplands, Grasslands, and Cropland Mosaics. Cropland Mosaics are lands with a mosaic of croplands less than 60 % of the landscape (Friedl et al., 2002). Because urban environments can also be sources of anthropogenic dust, we get information about the extent of urban areas from the Global Rural-Urban Mapping Project (GRUMP) v1 (Schneider et al., 2010) dataset. In Fig. 1, we summarize the geographical distribution of the anthropogenic dust source types described above. The colors indicate the locations of the four different anthropogenic dust source types: red represents urban areas, orange represents grassland, yellow represents cropland, and green represents cropland mosaics. The four black rectangles denote four regions that will be emphasized later: East China, India, North America, and Africa.

### 2.3 Precipitation data

Anthropogenic dust emissions depend on soil moisture content and therefore on precipitation and climate state regime. In this study, we use precipitation as a proxy for climate state regime. The University of East Anglia Climate Research Unit (CRU) Global Climate Dataset provides the monthly mean precipitation climatologies for global land areas, excluding Antarctica (New et al., 1999), which is used in this study. The data set is based on analysis of over 4000 individual weather station records and is provided at 0.5° latitude and longitude resolution. The CRU Global Climate Dataset temperature and precipitation, estimates were made for 80–100 % of the land surface (Mitchell and Jones, 2005). In this study the monthly mean climatology was calculated relative to the average for the period 1961–1990.

## 3 Dust detection and identification methods

It is a challenge to distinguish the anthropogenic dust component from natural dust (Sagan et al., 1979; Sokolik and Toon, 1996) due to the indirect nature of the satellite-





ACPD
15, 10163–10198, 2015

based measurement data. In 2012, Ginoux et al. proposed a method to detect anthropogenic dust by using MODIS deep blue products, but MODIS, a passive instrument, has limited accuracy over relatively bright, land surfaces. In order to get more accuracy and comprehensive results, we developed a new method to separate natural and anthropogenic dust and assess anthropogenic impacts on dust emissions at the global scale by using CALIPSO measurements.

Figure 2 shows a schematic of dust sources and vertical and horizontal transport processes underlying our approach for separating anthropogenic dust from natural dust. The yellow dots represent dust aerosol in the atmosphere; the arrows and red wavy lines indicate lifting and turbulence, respectively. It illustrates that natural dust from deserts can undergo long-range transport to other regions by lifting through the planetary boundary layer (PBL) to the free troposphere, as confirmed by Chen et al. (2013). Horizontal transport of natural dust aerosols occurs mainly above the PBL (Jordan et al., 2010; Yu et al., 2012). Only a small amount of this dust enters and remains within the PBL. However, it is this fraction that may be most relevant to air quality (Yu et al., 2012). Dusts from other land surface types and pollution sources are predominately trapped in the PBL where industrial and commercial activities, except for air travel, are conducted (Stull, 1988, 2000). We go through four steps to discriminate anthropogenic dust from natural dust in the CALIPSO data. The first step is to detect the total dust load (both natural and anthropogenic). The second step is to determine the source region of the dust. The third step is to determine the height of PBL, and the final step is to determine which dust is anthropogenic dust i.e., that subset of the total dust within PBL.

## 3.1 Step 1: total dust detection

Aerosol subtypes are stored in the parameter "Feature Classification Flags" of CALIPSO VFM data. Therefore, dust aerosols are identified by Feature Classification Flags in this paper. We only use dust aerosol feature for which there is high confidence, i.e., absolute values of CAD score greater than 70. Then, dust aerosol extinction co-





ACPD
15, 10163–10198, 2015

efficients are integrated under the condition of extinctions QC = 0 and QC = 1, which are chosen from CALIPSO's aerosol profile product. Next, we calculated dust aerosol optical depth as well as dust column burden ($\mathrm{g\,m^{-2}}$) in Eq. (1).

### 3.2 Step 2: selection of source regions of anthropogenic dust

As stated previously, anthropogenic dust mainly comes from harvesting, ploughing, overgrazing, construction, traffic, etc. We assume that anthropogenic dust will typically be emitted from cropland, grasslands, and urban surfaces (referred to as "anthropogenic surface"), will have thinner dust aerosol layers, will be predominately trapped in PBL, and will rarely be lifted into the free atmosphere by wind and turbulence. Therefore, we restrict our source regions to the urban, grassland, cropland, and mosaic cropland surfaces from the MODIS and GRUMP datasets, as seen in Fig. 1.

### 3.3 Step 3: determination of PBL height

In this step, we determine and used PBL height to exclude long-distance transport of dust aerosol from dust sources above the anthropogenic surface described above, so it is important to accurately determine PBL height to separate out the anthropogenic dust.

We can use CALIPSO to determine PBL height because, in general, the PBL is capped by a temperature inversion that tends to trap moisture and aerosols. The gradient of backscatter seen by lidar is almost always associated with this temperature inversion and the simultaneous decrease in moisture content (Palm et al., 1998; Melfi et al., 1985). Thus, the definition of the PBL top as the location of the maximum aerosol scattering gradient is analogous to the more conventional thermodynamic definition. McGrath-Spangler and Denning (2012) revealed that the Modern-era Retrospective Analysis for Research and Applications (MERRA) PBL depths are within 25 % of the estimates derived from the maximum standard technique (Jordan et al., 2010) by





ACPD
15, 10163–10198, 2015

CALIPSO, which is better than radiosonde estimates of space/time average PBL depth (Angevine et al., 1994).

We modified the maximum standard technique developed by Jordan et al. (2010) and derived global PBL heights using this method, which are consistent with results of McGrath-Spangler and Denning (2012). And, we found that this technique compared favorably to the ground-based lidar at the Semi-Arid Climate and Environment Observatory of Lanzhou University (SACOL) with a correlation coefficient of 0.73 (Liu et al., 2014).

### 3.4 Step 4: identification of anthropogenic dust within PBL

The final step is to identify the anthropogenic dust within the PBL. Two parameters, the layer integrated depolarization ratio $\delta'$ and the layer integrated attenuated backscatter coefficient $\gamma'$, can be used to explore the difference in optical properties between natural dust and anthropogenic dust. As an illustration of the process and resulting output of this step, we chose two typical areas based on dust optical depth ($\tau$), population density, and land cover distribution, to represent sources of anthropogenic dust (North China: 35.0–39.0° N, 114.0–118.0° E) and natural dust source (Taklimakan: 38.0–40.0° N, 78.0–83.0° E). Because spring (March to May) is the most active season for dust emission in the Taklimakan region, 4 years (2007 through 2010) of spring, daytime CALIPSO measurements were used to look at the optical properties of natural dust aerosol. Because anthropogenic dust has little seasonal dependence and natural dust is at its minimum in autumn, we used 4 years of autumn measurements to look at the optical properties of anthropogenic dust. For these two seasons, the statistical distribution of the layer-integrated $\delta'$ and $\gamma'$ for both anthropogenic dust and natural dust from the entire profile and within the PBL, respectively was constructed by summing occurrences within grid boxes of $\Delta\delta' - \Delta\gamma'$ measuring 0.01-by-0.001 $sr^{-1}$.

In Fig. 3a, we can see that a threshold of $\delta' = 0.25$ can be used to discriminate dust based on the entire profiles from the Taklimakan and North China. Figure 3b shows that a lower threshold of $\delta' = 0.23$ can be used to separate anthropogenic dust from





ACPD
15, 10163–10198, 2015

natural dust within the PBL. The larger threshold value for the entire profile compared to the PBL is mainly due to the fact that natural dust transport above the PBL in North China leads to a larger depolarization ratio. Furthermore, anthropogenic dust has lower layer-integrated attenuated backscatter is because anthropogenic dust produced by human activities and generally mixed with other type aerosols within the PBL, which has lower non-spherical. Natural dust is more non-spherical than anthropogenic dust, so anthropogenic dust has lower layer-integrated depolarization ratio than natural dust.

Therefore, anthropogenic dust could be accurately distinguished from natural dust by the above steps. Inevitably, there are some misclassifications of anthropogenic and natural dust owing to anthropogenic dust mixed with natural dust above and below the PBL. This problem should be kept in mind in the following results and discussion. Quantitatively, ~ 9.6 % of anthropogenic dust is misclassified as natural dust and 8.7 % of natural dust is misclassified as anthropogenic dust within the PBL along with the anthropogenic dust, respectively.

A detailed flow chart of the anthropogenic dust detection algorithm is shown in Fig. 4.

## 4 Calculation of anthropogenic dust column burden (DCB)

Based on the detection methods described above, we are able to identify anthropogenic dust and calculate anthropogenic dust column burden as a subset of the global dust column burden. First, we used the dust extinction coefficient through the parameter "Atmospheric Volume Description" which is used to discriminate between aerosols and clouds in the CALIPSO Level 2 aerosol extinction profile products. Then, dust extinction coefficients with higher confidence levels ($|CAD| \geq 70$) (Liu et al., 2010) and quality-control ($QC = 0$ or $QC = 1$) based on the study of Chen et al. (2013) were selected. Therefore, dust optical depth (DOD, $\tau$) can be calculated by integrating the CAD and QC quality-controlled extinction coefficient of dust aerosol over the height of the dust layer.



Discussion Paper | Discussion Paper | Discussion Paper | Discussion Paper |

ACPD
15, 10163–10198, 2015

Detection of anthropogenic dust using CALIPSO lidar measurements

J. Huang et al.

After calculating global total DOD ($\tau_t$) and anthropogenic DOD ($\tau_a$) from the CALIPSO profile products between January 2007 and December 2010, we were able to calculate dust column burdens. The conversion from dust optical depth ($\tau$) to dust column mass burden ($M$) was calculated following Ginoux et al. (2001):

$$M = \frac{4}{3}\frac{\rho r_{\mathrm{eff}}}{Q_{\mathrm{ext}}}\tau = \frac{1}{\varepsilon}\tau \tag{1}$$

Where, $r_{\mathrm{eff}}$ is the dust effective radius, $\rho$ is the density of dust, $Q_{\mathrm{ext}}$ is the dust extinction efficiency, and $\varepsilon$ is the mass extinction efficiency. Ginoux et al. (2012) used daily global DOD from MODIS deep blue aerosol products and converted it into column burden. In this study, we follow those empirical values taken by Ginoux et al. (2012) and assume $r_{\mathrm{eff}} = 1.2\,\mu\mathrm{m}$, $\rho = 2600\,\mathrm{kg\,m^{-3}}$, $Q_{\mathrm{ext}} = 2.5$, $\varepsilon = 0.6\,\mathrm{m^2\,g^{-1}}$, and $\tau$ is the dust optical depth derived from the CALIPSO retrievals.

## 5 Results

The global distribution of seasonal mean, total DOD with $1.25^\circ \times 1.25^\circ$ resolution derived from CALIPSO measurements for 2007 through 2010 are presented in Fig. 5, which shows that dust covers a larger area in the Northern Hemisphere than Southern Hemisphere. The Taklimakan and Gobi deserts in China (Qian et al., 2002) and the deserts on the Indian Subcontinent (Middleton, 1986) are major dust source regions, subordinate only to North Africa and the Arabian Peninsula (Prospero et al., 2002; Liu et al., 2008). These major dust sources are located in the broad “dust belt” which stretch from the western coast of North Africa to China, covering the Sahara and Sahel regions, the Arabian Peninsula, northern India, the Tarim Basin and Gobi desert (Herman et al., 1997; Prospero et al., 2002; Liu et al., 2008), and are usually associated with topographical basins in these arid regions, on land adjacent to high mountainous or plateau regions or in intermountain basins as discussed in detail by Prospero et al. (2002). In these source regions the annual rainfall is generally low,





ACPD
15, 10163–10198, 2015

less than 200–250 mm. Significant seasonal variation of DOD is illustrated in Fig. 5a–d. During the spring and summer, dust outbreaks are most active in this dust belt. In North Africa and the Arabian Peninsula, summer is the more active season. Spring is the more active season in the Indian Subcontinent and Taklimakan region. In the Arabian Peninsula, Indian Subcontinent and Taklimakan, dust activities weaken rapidly in autumn, reaching a minimum in winter. Figure 5 clearly shows a main dust transport pathway: the trans-Atlantic transport of North African dust which stretches the "dust belt" out toward the America continent. The North Africa dust is transported across the Atlantic all year long with strong seasonal dependencies of which spring and summer are the most active and autumn the least active. And the Hexi Corridor as a minor transport pathway in East Asia even though it is clearly subordinate to the North Atlantic pathway. This is path shown in Fig. 5, too, even though it is not as strong or clear as the North Atlantic pathway.

Using Eq. (1), we calculated the global annual mean total dust column burden (DCB) to be 79.3 Tg. The global seasonal mean values, which are 81.5 Tg (spring), 81.0 Tg (summer), 73.7 Tg (autumn) and 77.5 Tg (winter), show that dust burden in the atmosphere is greater in the spring and summer. Huneeus et al. (2011) pointed out that the global annual mean dust burden values from 14 models range from 6.8 to 29.5 Tg, which is far lower than our results. A possible reason is for this difference is that air masses with pollution aerosol and dust are included in our results which account for episodes of dust mixed with biomass burning smoke, instances of dust mixed with urban pollution and dust mixed with sea-salt aerosol (Omar et al., 2009). In these cases the depolarization ratio is dominated by the dust component and the entire mixture will be classified as dust and the DCB will be biased high.

Figure 6 illustrates the global distribution of seasonal mean anthropogenic DCBs. Global seasonal mean anthropogenic DCBs are 7.0 Tg (spring), 6.9 Tg (summer), 6.1 Tg (autumn), and 6.0 Tg (winter), respectively. This is different than the seasonal pattern of natural dust optical depth ($\tau_n$), with anthropogenic DCB showing minimal seasonal variation owing to anthropogenic dust emissions which are controlled by human activities and urban pollutants. Larger dust column burdens occurred in East China, India, and North Africa for all seasons, which are related to higher population densities in the East China and India regions and biomass burning throughout the year in Africa due to farmers preparing for the agricultural season and grazing areas (Justice et al., 1996). The global annual mean anthropogenic DCB is 6.7 Tg, which accounts for 8.4 % of the total global dust column burden. In order to avoid the impact of dust on the ocean, we only calculated global continent dust aerosols and found that anthropogenic dust sources account for 24.8 % of total continental dust sources (including polluted dust). There are mainly two reasons for the difference with Ginoux et al. (2012): MODIS deep blue algorithm only retrieved dust optical depth over bright surface (excluding forest and ocean) lead to a lower dust burden, and MODIS data products have not vertical information which cannot extract natural dust from deserts transported to anthropogenic surface bring with a bigger result.

Figure 7 shows the global distribution of the percentage of anthropogenic dust within the total dust column burden over land. This illustrates the significance of dust related with human activities in many local regions. Several features are evident in these maps. Eastern North America, India, East China and Europe show high percentages, larger than 60 %, which correspond to highly populated or intensively cultivated agricultural regions. Lower percentages occur over Western North America, North Africa, etc.

Figure 8 shows a comparison of global dust column burdens as function of climatological mean precipitation for the spring, summer, autumn, and winter seasons. Although precipitation is related to surface temperature, the long-term mean precipitation is the simplest index for classifying climate regions. The mean precipitation varies spatially from less than 100 $\mathrm{mm\,yr^{-1}}$ to a maximum of 2000 $\mathrm{mm\,yr^{-1}}$ in Fig. 8, and the interval value is 100 $\mathrm{mm\,yr^{-1}}$. The average anthropogenic dust column burdens corresponding to the precipitation intervals are plotted for each interval. From Fig. 8 we found that anthropogenic dusts mainly come from semi-arid and semi-wet regions over the whole year. The semi-arid regions are transition zones between arid and semi-wet regions, which are defined as areas where precipitation is less than potential evapora-





ACPD
15, 10163–10198, 2015

tion, and are characterized by high temperatures (30–45 °C) during the hottest months. Annual mean precipitation ranges from 200 to 600 mm yr$^{-1}$ in semi-arid regions. Semi-wet regions cover considerable parts of eastern North America, Europe, and Central China with precipitation ranging from 600 to 800 mm yr$^{-1}$. Total anthropogenic DCB is larger in spring and summer than in autumn and winter. This difference is most significant in arid regions. There is almost no anthropogenic dust observed in arid regions due to minimal agricultural and human activities and urban pollutions. Table 1 shows annual mean anthropogenic DOD ($\tau_a$), total area, total anthropogenic DCB and the percent contribution to total DCB from wet, combined semi-arid and semi-wet, and arid regions. In wet regions the mean DOD is 0.12 and the anthropogenic contribution to the total DCB in wet regions is 80.3 %. This is larger than the respective anthropogenic contributions in combined semi-arid and semi-wet, and arid regions, revealing that anthropogenic dust plays an important role on total dust because the frequency of total natural dust events (suspended dust, blowing dust, and dust storms) is lower in wet regions. A statistical result of Table 1 suggests that anthropogenic dust aerosols from the combined semi-arid and semi-wet regions contribute 52.5 % to the total anthropogenic dust aerosol over all three regions. The more frequent occurrence of anthropogenic dust emissions over semi-wet and semi-arid may be related to the heavier human activity and poor ecological practices in that region.

Figure 9 shows the regional distribution of annual mean anthropogenic dust column burden derived from CALIPSO measurements in four regions: East China, India, North America and North Africa. Table 2 lists their latitude and longitude ranges, the area and percent of each region that is considered to contribute to anthropogenic dust emissions and the annual mean anthropogenic DCB of the regions. In India, anthropogenic dust sources occupy are distributed relatively evenly over the region; the anthropogenic dust source area is 70.2 % of the total area which is characterized by intense agricultural and human activities (Prasad et al., 2007). For North Africa, we also note in Figs. 9 and 10 that the southern Sahel dust sources are overwhelmingly anthropogenic, are associated with biomass burning aerosols, and there is a clear separation between natural





ACPD
15, 10163–10198, 2015

dust sources in the Sahara and anthropogenic dust in the southern Sahel. Compared with natural dust source areas, anthropogenic dust source areas only occupy 21.5 %. Figure 9 also shows that anthropogenic dust sources are mostly confined to areas in the northeast China, the North China Plain, and Inner Mongolia in East China. The largest anthropogenic DCBs are located over the North China Plain. This is also consistent with the conclusions of Wang et al. (2006), who find that dust storm frequency does not exceed 8 days per year in northern China, even where there are high levels of human activity. In Mongolia, there are dozens of small anthropogenic dust sources associated with pasturelands or grasslands. Most dust sources over North America are centered in two eastern areas, the Great Plains and the Great Basin which are separated by the continental divide. A major difference from the results of Ginoux et al. (2012) is that on the east side of the divide the anthropogenic and natural dust sources are heavily intertwined and on the west side of the divide sources are essentially anthropogenic. The largest anthropogenic DCBs are distributed over southeast of North America.

A histogram illustrating the relative contribution of anthropogenic and natural dust sources over anthropogenic dust source surfaces for the four study regions is shown in Fig. 10. Annual mean anthropogenic DCB values range from 0.42 $g\,m^{-2}$ with maximum in India to 0.12 $g\,m^{-2}$ with minimum in North America, including 0.23 $g\,m^{-2}$ in East China and 0.24 $g\,m^{-2}$ in North Africa. The anthropogenic dust contributions to the regional emission from East China and India are 91.8 and 76.1 %, followed by North America with 73.9 %, respectively. There is a possible explanation of the above phenomenon in that East China and India with larger population densities are characterized by more intense agricultural and human activities.

## 6 Discussion and conclusions

Emission of soil and mineral dust particles from the earth's surface is a small scale process that has global consequences (Okin et al., 2011), such as cloud formation





ACPD
15, 10163–10198, 2015

(Huang, 2006a, 2010), anthropogenic carbon dioxide emission, snow albedo change (Huang et al., 2011), and land use change (Sokolik et al., 2011). Dust emissions are affected by climate variability and in turn can impact climate, air quality, and human health (Ginoux et al., 2012). Global dust aerosols not only contain locally emitted, anthropogenic aerosols (agricultural dust, industrial black carbon, and other anthropogenic aerosols), but also include natural dust from deserts. Dust emissions that result from anthropogenic activities could account for a large proportion of global dust emission that has been quantified but with large uncertainty (Sokolik and Toon, 1996). In this paper, we have developed an algorithm to detect anthropogenic dust based on CALIPSO measurements and the MODIS land cover dataset. From this, the contribution of anthropogenic dust to the total global dust load was determined.

We conducted a case-study to test our algorithm using CALIPSO data for the Taklimakan and North China, known natural and anthropogenic dust source regions respectively. From this we found that anthropogenic dust has a layer-integrated depolarization ratio that is less than that for natural dust. This difference is mainly from the result of anthropogenic dust produced by human activities being generally mixed with other type aerosols within the PBL, thus being more spherical than natural dust. However, there are some misclassifications that should be kept in mind for the results. Approximately 9.6 % of anthropogenic dust is misclassified as natural dust and 8.7 % of natural dust is misidentified as anthropogenic dust within the PBL. The local anthropogenic dust aerosol due to human activity, such as agriculture and industrial activity, accounts for 25 % contribution to the global continent dust load. The anthropogenic dust aerosols mainly come from semi-arid and semi-wet region, occupying more than 52 % to the total anthropogenic dust aerosols.

An analysis of sources over four different continental regions reveals regional characteristics. Annual mean anthropogenic DCB value varies from 0.12 $\mathrm{g\,m^{-2}}$ in North America to 0.42 $\mathrm{g\,m^{-2}}$ in India. Considering the mean DCB in four regions, the greatest burden of anthropogenic dust occurs over India and the greatest burden of natural dust occurs over Africa. On a percentage basis, anthropogenic dust is greatest over East





ACPD
15, 10163–10198, 2015

China and natural dust over Africa. Some studies have confirmed that human activities, mainly farming, overgrazing, and water usage, have likely been responsible for the expansion of dust sources in northern China and India (Xuan and Sokolik, 2002; Prasad et al., 2007). Igarashi et al. (2011) add that drought has been also a contributing factor. Gong et al. (2004) showed that although desertification has increased by only a few percent in China, it has generated disproportionately large areas of enhanced dust emissions. The relationship between population density and anthropogenic DCB from our four study regions further supports the above results. In this paper, anthropogenic dust mainly comes from cropland, urban, and pasture. Anthropogenic dust from intermittent dry lake basins is not considered. A major uncertainty in these results comes from the assumption of a single value for mass extinction efficiency in Eq. (1) that was used in this paper; this parameter probably varies between the different regions. To reduce this uncertainty, it will be necessary to determine different mass extinction efficiency for the natural and anthropogenic dusts from different regions. What's more, the local anthropogenic dusts also make some contribution to local climate, air quality, and human health. Therefore, it is necessary to further investigate the regional interaction among aerosol-cloud-precipitation processes and improve the parameterization of local air pollution effects (Huang et al., 2006a, b, 2010, 2014; Li et al., 2011).

*Acknowledgement.* Supported by the National Basic Research Program of China (2012CB955301), National Sciences Foundation of China (41305026 & 41375032), the China 111 project (No. B 13045). CALIPSO data have been obtained from the Atmospheric Sciences Data Center (ASDC) a NASA Langley Research Center. The MODIS data were obtained from the NASA Earth Observing System Data and Information System, Land Processes Distributed Active Archive Center (LP DAAC) at the USGS Earth Resources Observation and Science (EROS) Center.





ACPD
15, 10163–10198, 2015

## References

Angevine, W. M., White, A. B., and Avery, S. K.: Boundary-layer depth and entrainment zone characterization with a boundary-layer profiler, Bound.-Lay. Meteorol., 68, 375–385, doi:10.1007/BF00706797, 1994.

Bullard, J. E., Harrison, S. P., Baddock, M., Drake, N. A., Gill, T. E., McTainsh, G. H., and Sun, Y.: Preferential dust sources: a geomorphological classification designed for use in global dust-cycle models, J. Geophys. Res., 116, F04034, doi:10.1029/2011JF002061, 2011.

Chen, S., Huang, J., Zhao, C., Qian, Y., Leung, L. R., and Yang, B.: Modeling the transport and radiative forcing of Taklimakan dust over the Tibetan Plateau: a case study in the summer of 2006, J. Geophys. Res., 118, 797–812, doi:10.1002/jgrd.50122, 2013.

Friedl, M. A., McIver, D. K., Hodges, J. C. F., Zhang, X. Y., Muchoney, D., Strahler, A. H., Woodcocka, C. E., Gopal, S., Schneider, A., Cooper, A., Baccini, A., Gao., F., and Schaaf, C.: Global land cover mapping from MODIS: algorithms and early results, Remote Sens. Environ., 83, 287–302, 2002.

Friedl, M. A., Sulla-Menashe, D., Tan, B., Schneider, A., Ramankutty, N., Sibley, A., and Huang, X.: MODIS Collection 5 global land cover: algorithm refinements and characterization of new datasets, Remote Sens. Environ., 114, 168–182, doi:10.1016/j.rse.2009.08.016, 2010.

Ginoux, P., Chin, M., Tegen, I., Prospero, J. M., Holben, B., Dubovik, O., and Lin, S. J.: Sources and distributions of dust aerosols simulated with the GOCART model, J. Geophys. Res., 106, 20255–20273, doi:10.1029/2000JD000053, 2001.

Ginoux, P., Prospero, J. M., Gill, T. E., Hsu, N. C., and Zhao, M.: Global-scale attribution of anthropogenic and natural dust sources and their emission rates based on MODIS Deep Blue aerosol products, Rev. Geophys., 50, RG3005, doi:10.1029/2012RG000388, 2012.

Gong, S., Zhang, X., Zhao, T., and Barrie, L.: Sensitivity of Asian dust storm to natural and anthropogenic factors, Geophys. Res. Lett., 31, L07210, doi:10.1029/2004GL019502, 2004.

Herman, J., Bhartia, P., Torres, O., Hsu, C., Seftor, C., and Celarier, E.: Global distribution of UV-absorbing aerosols from Nimbus 7/TOMS data, J. Geophys. Res., 102, 16911–16922, doi:10.1029/96JD03680, 1997.

Hu, Y., Vaughan, M., Liu, Z., Lin, B., Yang. P., Flittner, D., Hunt, B., Kuehn, R., Huang, J., Wu, D., Rodier, S., Powell, K., Trepte, C., and Winker, D.: The depolarization-attenuated backscatter relation: CALIPSO lidar measurements vs. theory, Opt. Express, 15, 5327–5332, 2007a.

Hu, Y., Vaughan, M., McClain, C., Behrenfeld, M., Maring, H., Anderson, D., Sun-Mack, S., Flittner, D., Huang, J., Wielicki, B., Minnis, P., Weimer, C., Trepte, C., and Kuehn, R.: Global statistics of liquid water content and effective number concentration of water clouds over ocean derived from combined CALIPSO and MODIS measurements, Atmos. Chem. Phys., 7, 3353–3359, doi:10.5194/acp-7-3353-2007, 2007b.

Hu, Y., Winker, D., Vaughan, M., Lin, B., Omar, A., Trepte, C., Flittner, D., Yang, P., Nasiri, S. L., Baum, B., Sun, W., Liu, Z., Wang, Z., Young, S., Stamnes, K., Huang, J., Kuehn, R., and Holz, R.: CALIPSO/CALIOP Cloud Phase Discrimination Algorithm, J. Atmos. Ocean. Tech., 26, 2293–2309, 2009.

Huang, J., Lin, B., Minnis, P., Wang, T., Wang, X., Hu, Y., Yi, Y., and Ayers, J. R.: Satellite-based assessment of possible dust aerosols semi-direct effect on cloud water path over East Asia, Geophys. Res. Lett., 33, L19802, doi:10.1029/2006GL026561, 2006a.

Huang, J., Minnis, P., Lin, B., Wang, T., Yi, Y., Hu, Y., Sun-Mack, S., and Ayers, K.: Possible influences of Asian dust aerosols on cloud properties and radiative forcing observed from MODIS and CERES, Geophys. Res. Lett., 33, L06824, doi:10.1029/2005GL024724, 2006b.

Huang, J., Minnis, P., Yan, H., Yi, Y., Chen, B., Zhang, L., and Ayers, J. K.: Dust aerosol effect on semi-arid climate over Northwest China detected from A-Train satellite measurements, Atmos. Chem. Phys., 10, 6863–6872, doi:10.5194/acp-10-6863-2010, 2010.

Huang, J., Fu, Q., Zhang, W., Wang, X., Zhang, R., Ye, H., and Warren, S. G.: Dust and black carbon in seasonal snow across northern China, B. Am. Meteorol. Soc., 92, 175–181, doi:10.1175/2010BAMS3064.1, 2011.

Huang, J., Wang, T., Wang, W., Li, Z., and Yan, H.: Climate effects of dust aerosols over East Asian arid and semi-arid regions, J. Geophys. Res., 119, 11398–11416, doi:10.1002/2014JD021796, 2014.

Huneeus, N., Schulz, M., Balkanski, Y., Griesfeller, J., Prospero, J., Kinne, S., Bauer, S., Boucher, O., Chin, M., Dentener, F., Diehl, T., Easter, R., Fillmore, D., Ghan, S., Ginoux, P., Grini, A., Horowitz, L., Koch, D., Krol, M. C., Landing, W., Liu, X., Mahowald, N., Miller, R., Morcrette, J.-J., Myhre, G., Penner, J., Perlwitz, J., Stier, P., Takemura, T., and Zender, C. S.: Global dust model intercomparison in AeroCom phase I, Atmos. Chem. Phys., 11, 7781–7816, doi:10.5194/acp-11-7781-2011, 2011.

Igarashi, Y., Fujiwara, H., and Jugder, D.: Change of the Asian dust source region deduced from the composition of anthropogenic radionuclides in surface soil in Mongolia, Atmos. Chem. Phys., 11, 7069–7080, doi:10.5194/acp-11-7069-2011, 2011.





ACPD
15, 10163–10198, 2015

Detection of anthropogenic dust using CALIPSO lidar measurements

J. Huang et al.

Jordan, N. S., Hoff, R. M., and Bacmeister, J. T.: Validation of Goddard Earth Observing System-version 5 MERRA planetary boundary layer heights using CALIPSO, J. Geophys. Res., 115, D24218, doi:10.1029/2009JD013777, 2010.
Justice, C., Kendall, J., Dowty, P., and Scholes, R.: Satellite remote sensing of fires during the SAFARI campaign using NOAA advanced very high resolution radiometer data, J. Geophys. Res., 101, 23851–23863, doi:10.1029/95JD00623, 1996.
Li, Z., Li, C., Chen, H., Tsay, S.-C., Holben, B., Huang, J., Li, B., Maring, H., Qian, Y., Shi, G., Xia, X., Yin, Y., Zheng, Y., and Zhuang, G.: East Asian Studies of Tropospheric Aerosols and their Impact on Regional Climate (EAST-AIRC): an overview, J. Geophys. Res., 116, D00K34, doi:10.1029/2010JD015257, 2011.
Liu, D., Wang, Z., Liu, Z., Winker, D., and Trepte, C.: A height resolved global view of dust aerosols from the first year CALIPSO lidar measurements, J. Geophys. Res., 113, D16214, doi:10.1029/2007JD009776, 2008.
Liu, Z., Vaughan, M. A., Winker, D. M., Hostetler, C. A., Poole, L. R., Hlavka, D., Hart, W., and McGill, M.: Use of probability distribution functions for discriminating between cloud and aerosol in lidar backscatter data, J. Geophys. Res., 109, D15202, doi:10.1029/2004JD004732, 2004.
Liu, Z., Liu, D., Huang, J., Vaughan, M., Uno, I., Sugimoto, N., Kittaka, C., Trepte, C., Wang, Z., Hostetler, C., and Winker, D.: Airborne dust distributions over the Tibetan Plateau and surrounding areas derived from the first year of CALIPSO lidar observations, Atmos. Chem. Phys., 8, 5045–5060, doi:10.5194/acp-8-5045-2008, 2008.
Liu, Z., Kuehn, R., Vaughan, M., Winker, D., Omar, A., Powell, K., Trepte, C., Hu, Y., and Hostetler, C.: The CALIPSO cloud and aerosol discrimination: Version 3 algorithm and test results, 25th International Laser Radar Conference (ILRC), St. Petersburg, Russia, 5–9, 2010.
Liu, J., Huang, J., Chen, B., Zhou, T., Yan, H., Jin, H., Huang, Z., and Zhang, B.: Comparisons of PBL heights derived from CALIPSO and ECMWF reanalysis data over China, J. Quant. Spectrosc. Ra., 153, 102–112, doi:10.1016/j.jqsrt.2014.10.011, 2014.
Loveland, T. R. and Belward, A. S.: The IGBP-DIS global 1 km landcover data set, DISCover: first results, Int. J. Remote Sens., 18, 3289–3295, doi:10.1080/014311697217099, 1997.
Mahowald, N. M. and Luo, C.: A less dusty future?, Geophys. Res. Lett., 30, 1903, doi:10.1029/2003GL017880, 2003.

Mahowald, N. M., Zender C. S., Luo C., Savoie D., Torres O., and Corral del, J.: Understanding the 30-year Barbados desert dust record, J. Geophys. Res., 107, D21, doi:10.1029/2002JD002097, 2002.
McGrath-Spangler, E. L. and Denning, A. S.: Estimates of North American summertime planetary boundary layer depths derived from space-borne lidar, J. Geophys. Res., 117, D15101, doi:10.1029/2012JD017615, 2012.
Melfi, S., Spinhirne, J., Chou, S., and Palm, S.: Lidar observations of vertically organized convection in the planetary boundary layer over the ocean, J. Clim. Appl. Meteorol., 24, 806–821, 1985.
Middleton, N.: A geography of dust storms in south-west Asia, J. Climate, 6, 183–196, doi:10.1002/joc.3370060207, 1986.
Mielonen, T., Arola, A., Komppula, M., Kukkonen, J., Koskinen, J., de Leeuw, G., and Lehtinen, K.: Comparison of CALIOP level 2 aerosol subtypes to aerosol types derived from AERONET inversion data, Geophys. Res. Lett., 36, L18804, doi:10.1029/2009GL039609, 2009.
Mitchell, T. D. and Jones, P. D.: An improved method of constructing a database of monthly climate observations and associated high-resolution grids, Int. J. Climatol., 25, 693–712, doi:10.1002/joc.1181, 2005.
Moulin, C. and Chiapello, I.: Evidence of the control of summer atmospheric transport of African dust over the Atlantic by Sahel sources from TOMS satellites (1979–2000), Geophys. Res. Lett., 31, L02107, doi:10.1029/2003GL018931, 2004.
Mulitza, S., Heslop, D., Pittauerova, D., Fischer, H. W., Meyer, I., Stuut, J.-B., Zabel, M., Mollenhauer, G., Collins, J. A., and Kuhnert, H.: Increase in African dust flux at the onset of commercial agriculture in the Sahel region, Nature, 466, 226–228, doi:10.1038/nature09213, 2010.
New, M., Hulme, M., and Jones, P.: Representing Twentieth-Century Space–Time Climate Variability, Part I: Development of a 1961–90 mean monthly terrestrial climatology, J. Climate, 12, 829–856, 1999.
Okin, G. S., Bullard, J. E., Reynolds, R. L., Ballantine, J. A. C., Schepanski, K., Todd, M. C., Belnap, J., Baddock, M. C., Gill, T. E., and Miller, M. E.: Dust: Small-scale processes with global consequences, Eos, Transactions American Geophysical Union, 92, 241–242, doi:10.1029/2011EO290001, 2011.





ACPD
15, 10163–10198, 2015

Omar, A. H., Winker, D. M., Kittaka, C., Vaughan, M. A., Liu, Z., Hu, Y., Trepte, C. R., Rogers, R. R., Ferrare, R. A., and Lee, K.-P.: The CALIPSO automated aerosol classification and lidar ratio selection algorithm, J. Atmos. Ocean. Tech., 26, 1994–2014, doi:10.1175/2009JTECHA1231.1, 2009.

Palm, S. P., Hagan, D., Schwemmer, G., and Melfi, S.: Inference of marine atmospheric boundary layer moisture and temperature structure using airborne lidar and infrared radiometer data, J. Appl. Meteorol., 37, 308–324, doi:10.1175/1520-0450-37.3.308, 1998.

Prasad, A. K., Singh, S., Chauhan, S., Srivastava, M. K., Singh, R. P., and Singh, R.: Aerosol radiative forcing over the Indo-Gangetic plains during major dust storms, Atmos. Environ., 41, 6289–6301, doi:10.1016/j.atmosenv.2007.03.060, 2007.

Prospero, J. M., Ginoux, P., Torres, O., Nicholson, S. E., and Gill, T. E.: Environmental characterization of global sources of atmospheric soil dust identified with the Nimbus 7 Total Ozone Mapping Spectrometer (TOMS) absorbing aerosol product, Rev. Geophys., 40, 2-1–2-31, doi:10.1029/2000RG000095, 2002.

Qian, W., Quan, L., and Shi, S.: Variations of the dust storm in China and its climatic control, J. Climate, 15, 1216–1229, 2002.

Sagan, C., Toon, O. B., Pollack, J. B.: Anthropogenic albedo changes and the earth's climate, Science, 206, 1363–1368, 1979.

Schneider, A., Friedl, M. A., and Potere, D.: Mapping global urban areas using MODIS 500 m data: new methods and datasets based on "urban ecoregions", Remote Sens. Environ., 114, 1733–1746, doi:10.1016/j.rse.2010.03.003, 2010.

Sokolik, I. N. and Toon, O. B.: Direct radiative forcing by anthropogenic airborne mineral aerosols, Nature, 381, 681–683, 1996.

Sokolik, I. N., Curry, J., and Radionov, V.: Interactions of Arctic aerosols with land-cover and land-use changes in Northern Eurasia and their role in the Arctic climate system, in: Eurasian Arctic Land Cover and Land Use in a Changing Climate, Focus on Eurasia, edited by: Gutman G. and Reissell, A. Springer, 2011.

Stull, R. B.: An Introduction to Boundary Layer Meteorology, Kluwer Academic, Dordrecht, 666 pp., 1988.

Stull, R. B.: Meteorology for Scientists and Engineers, Brooks/Cole, Pacific Grove, Calif., 2000.

Tegen, I. and Fung, I.: Contribution to the atmospheric mineral aerosol load from land surface modification, J. Geophys. Res., 100, 18707–18726, doi:10.1029/95JD02051, 1995.

Tegen, I., Werner, M., Harrison, S., and Kohfeld, K.: Relative importance of climate and land use in determining present and future global soil dust emission, Geophys. Res. Lett., 31, L05105, doi:10.1029/2003GL019216, 2004.

Vaughan, M., Young, S., Winker, D., Powell, K., Omar, A., Liu, Z., Hu, Y., and Hostetler, C.: Fully automated analysis of spacebased lidar data: an overview of the CALIPSO retrieval algorithms and data products, Proc. SPIE, 5575, 16–30, 2004.

Wang, X., Zhou, Z., and Dong, Z.: Control of dust emissions by geomorphic conditions, wind environments and land use in northern China: an examination based on dust storm frequency from 1960 to 2003, Geomorphology, 81, 292–308, doi:10.1016/j.geomorph.2006.04.015, 2006.

Winker, D. M., Hunt, W. H., and McGill, M. J.: Initial performance assessment of CALIOP, Geophys. Res. Lett., 34, L19803, doi:10.1029/2007GL030135, 2007.

Xuan, J. and Sokolik, I. N.: Characterization of sources and emission rates of mineral dust in Northern China, Atmos. Environ., 36, 4863–4876, doi:10.1016/S1352-2310(02)00585-X, 2002.

Young, S. A. and Vaughan, M. A.: The retrieval of profiles of particulate extinction from Cloud-Aerosol Lidar Infrared Pathfinder Satellite Observations (CALIPSO) Data: algorithm description, J. Atmos. Ocean. Tech., 26, 1105–1119, doi:10.1175/2008JTECHA1221.1, 2009.

Yu, H., Remer, L. A., Chin, M., Bian, H., Tan, Q., Yuan, T., and Zhang, Y.: Aerosols from overseas rival domestic emissions over North America, Science, 337, 566–569, doi:10.1126/science.1217576, 2012.





ACPD
15, 10163–10198, 2015

ACPD
15, 10163–10198, 2015

Detection of anthropogenic dust using CALIPSO lidar measurements

J. Huang et al.



**Table 1.** Summary of anthropogenic dust annual mean statistics by climate region. Anthropogenic dust optical depth (ADOD); total regional area; regional anthropogenic dust column burden (DCB) (and percent contribution by region); regional dust column burden (DCB); and percent contribution to regional DOD.

| Region | Mean anthropogenic DOD | Area ($km^2$) | Anthropogenic DCB (Tg) | DCB (Tg) | Contribution to regional DOD (%) |
|---|---|---|---|---|---|
| Wet | 0.12 | $1.77 \times 10^7$ | 2.48(41.2) | 3.09 | 80.3 |
| Semi-arid and semi-wet | 0.07 | $2.46 \times 10^7$ | 3.16(52.5) | 4.67 | 67.7 |
| Arid | 0.06 | $1.21 \times 10^6$ | 0.38(6.3) | 0.56 | 67.9 |

**Table 2.** Description of dust study areas. Latitude and longitude ranges; area and percent of the region considered to contribute to anthropogenic dust emissions; and annual mean anthropogenic dust column burden (ADCB) of the regions considered in this study.

| Region | Longitude Range | Latitude Range | Anthropogenic area $km^2$ (%) | Mean ADCB ($g\,m^{-2}$) |
|---|---|---|---|---|
| East China | 100.0–130.0° E | 25.0–50.0° N | $3.71 \times 10^6$ (63.0) | 0.17 |
| India | 60.0–90.0° E | 5.0–27.5° N | $1.98 \times 10^6$ (70.2) | 0.42 |
| North America | 135.0–65.0° W | 20.0–50.0° N | $5.56 \times 10^6$ (54.0) | 0.09 |
| North Africa | 20.0° W–35.0° E | 0.0–30.0° N | $3.40 \times 10^6$ (21.5) | 0.26 |

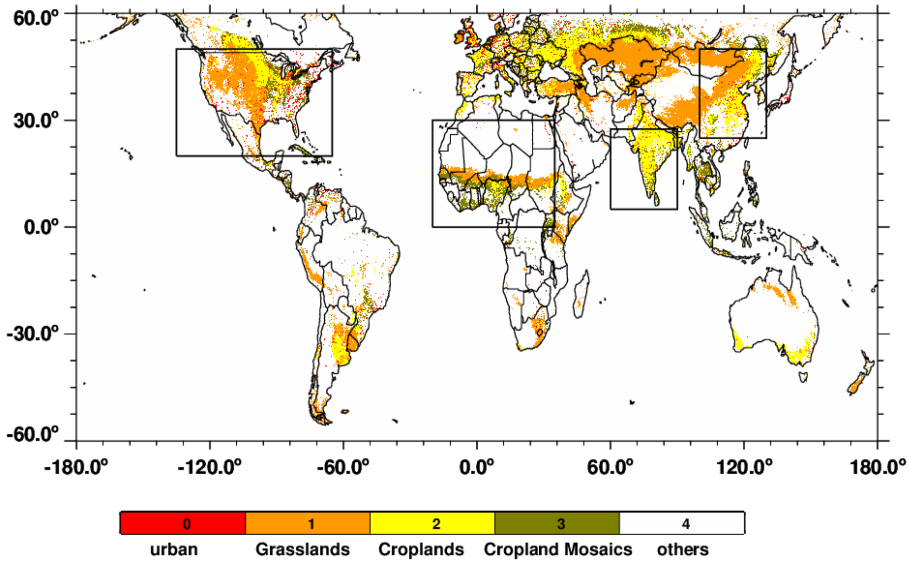


**Figure 1.** Global distribution of the land cover types for anthropogenic dust source types (including urban, cropland and grasslands) retrieved by combing MODIS and GRUMP data. The black rectangles denote four majors source regions studied: East China, India, North America, and Africa.





ACPD
15, 10163–10198, 2015

Detection of anthropogenic dust using CALIPSO lidar measurements

J. Huang et al.

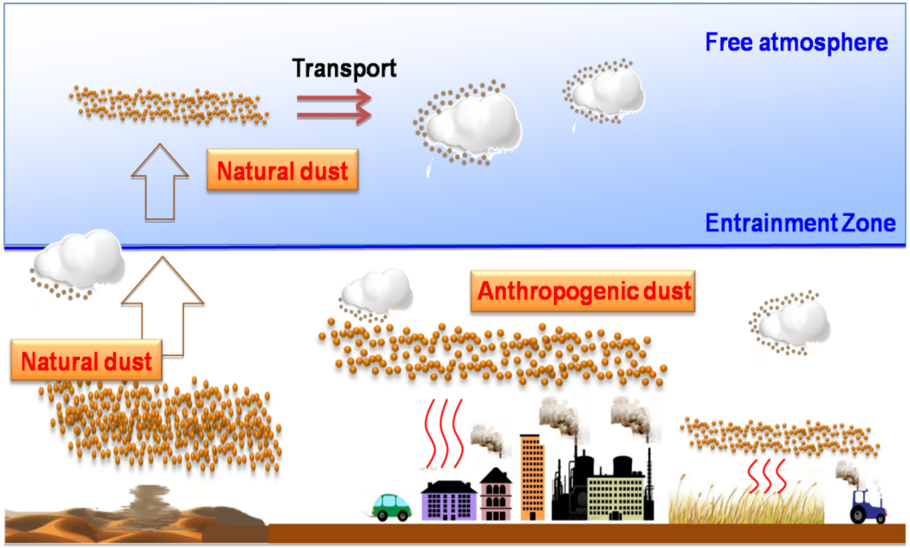


**Figure 2.** A conceptual schematic for sources and transport of dusts upon which the detection process of anthropogenic dust is based. The yellow dots represent dust aerosol in the atmosphere; the arrow and red wavy lines represent lifting and turbulence, respectively.





ACPD
15, 10163–10198, 2015

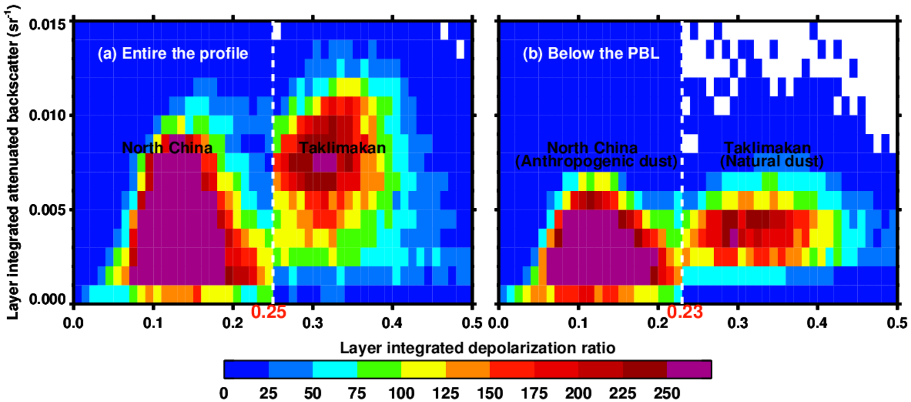


**Figure 3.** The relationship between the layer-integrated depolarization ratio $\delta'$ and the layer-integrated attenuated backscatter coefficient $\gamma'$ for North China and Taklimakan from the entire profile **(a)** and within the PBL **(b)**, respectively. The color of each pixel represents the frequency of occurrence for a $\Delta\delta' - \Delta\gamma'$ box measuring 0.01-by-0.001 sr$^{-1}$.





ACPD
15, 10163–10198, 2015

Detection of anthropogenic dust using CALIPSO lidar measurements

J. Huang et al.

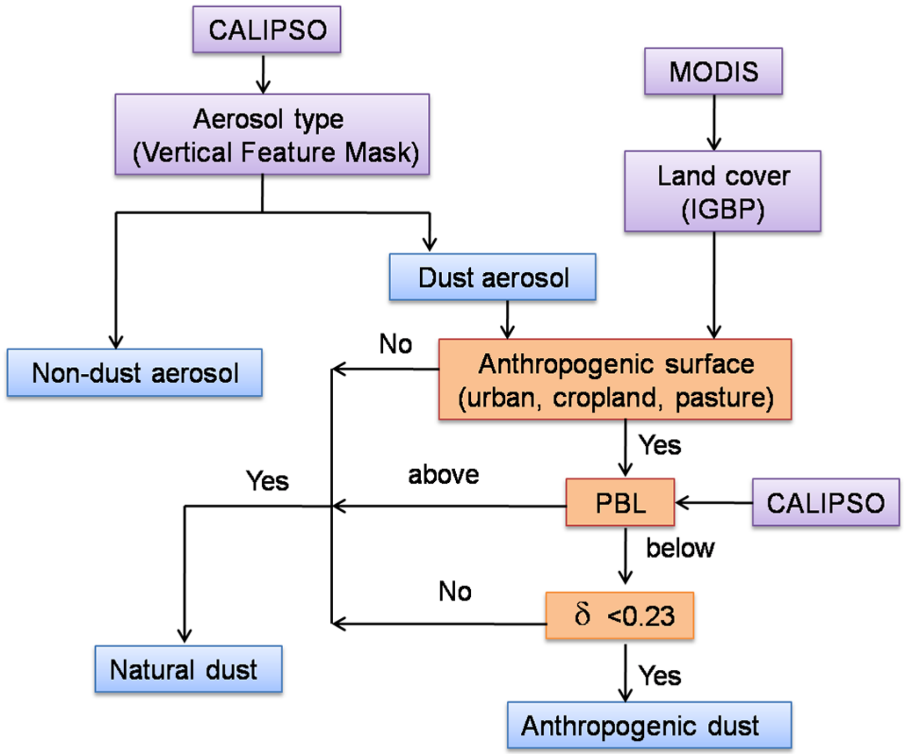


**Figure 4.** Flow chart of anthropogenic dust detection by combing CALIPSO and land cover dataset provided MODIS.





ACPD
15, 10163–10198, 2015

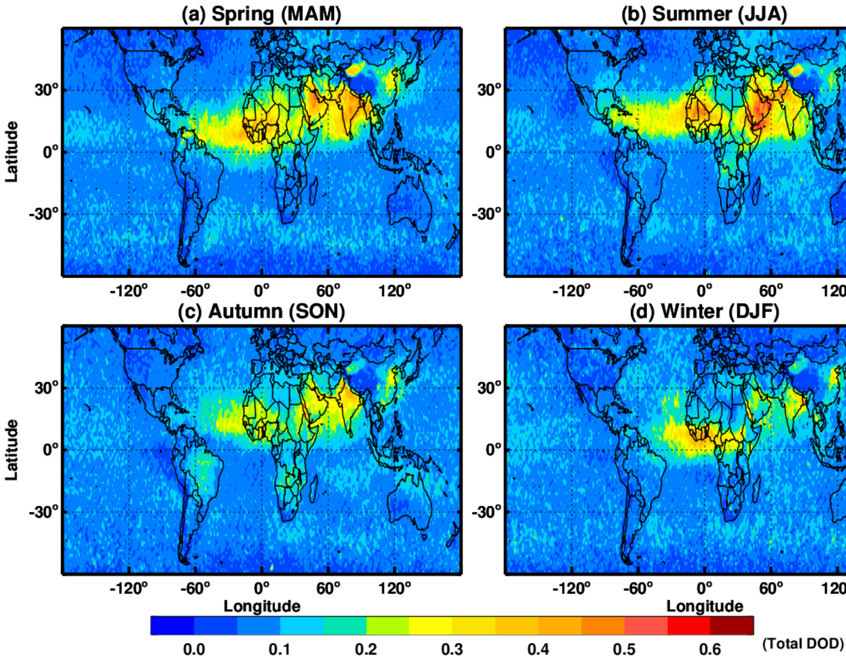


**Figure 5.** Global distributions of seasonal mean for total dust optical depth derived from CALIPSO measurements from 2007 through 2010.





ACPD
15, 10163–10198, 2015

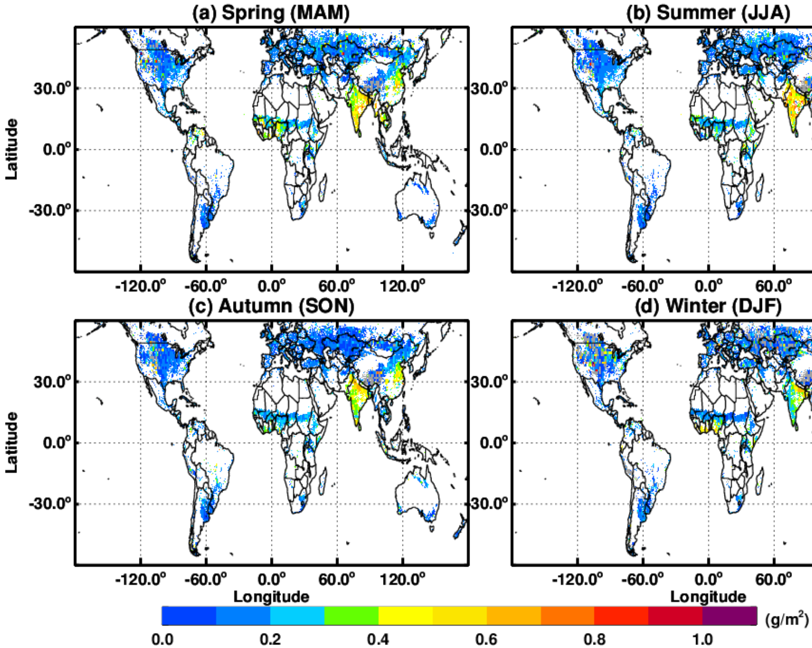


**Figure 6.** Global distribution of seasonal mean for anthropogenic dust column burden from 2007 through 2010.





ACPD
15, 10163–10198, 2015

Detection of anthropogenic dust using CALIPSO lidar measurements

J. Huang et al.

Title Page
Abstract Introduction
Conclusions References
Tables Figures
◂ ▸
Back Close
Full Screen / Esc
Printer-friendly Version
Interactive Discussion

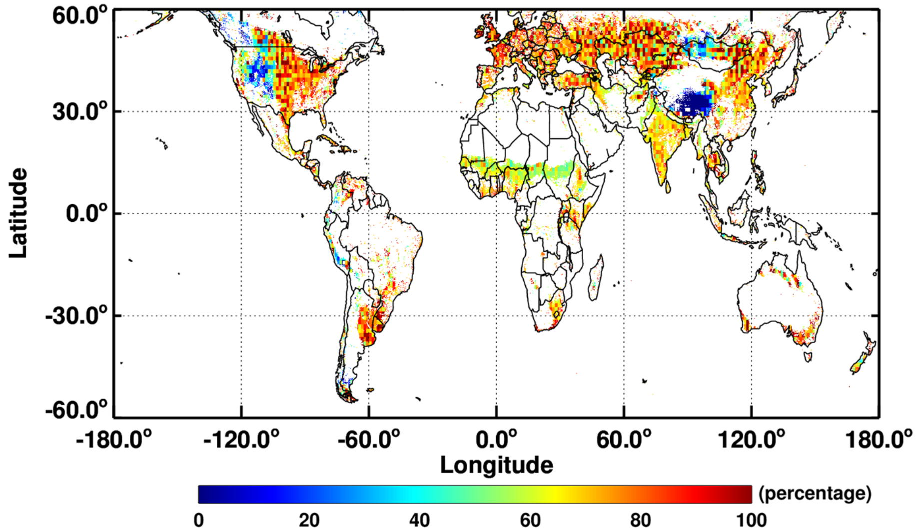


**Figure 7.** Global distribution of the percentage of anthropogenic dust within the total dust column burden.





ACPD
15, 10163–10198, 2015

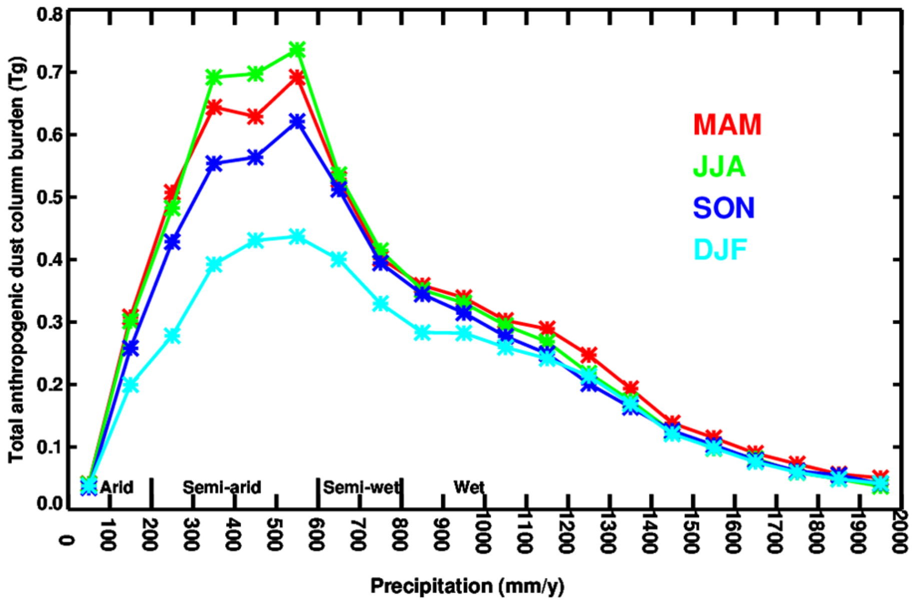


**Figure 8.** Comparisons of dust column burden over four seasons as a function of climatological mean precipitation. The precipitation interval is 100 mm $yr^{-1}$.





ACPD
15, 10163–10198, 2015

Detection of anthropogenic dust using CALIPSO lidar measurements

J. Huang et al.

Title Page
Abstract Introduction
Conclusions References
Tables Figures
◀I ▶I
◀ ▶
Back Close
Full Screen / Esc
Printer-friendly Version
Interactive Discussion

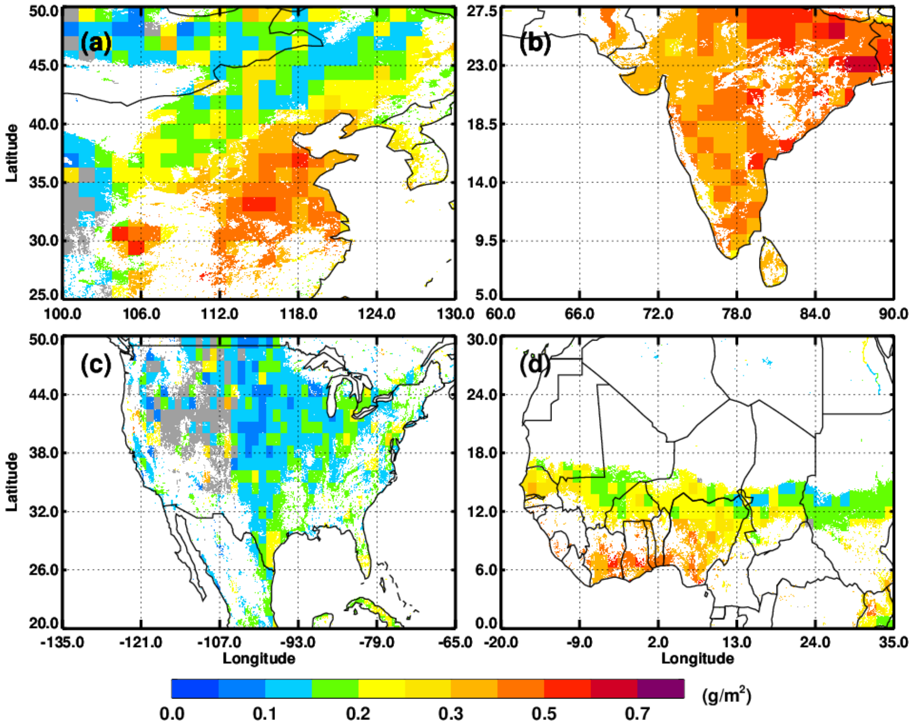


**Figure 9.** Regional distribution of annual mean anthropogenic dust column burden derived from CALIPSO measurements (2007 through 2010) for **(a)** East China, **(b)** India, **(c)** North America, and **(d)** North Africa.





ACPD
15, 10163–10198, 2015

**Detection of anthropogenic dust using CALIPSO lidar measurements**

J. Huang et al.

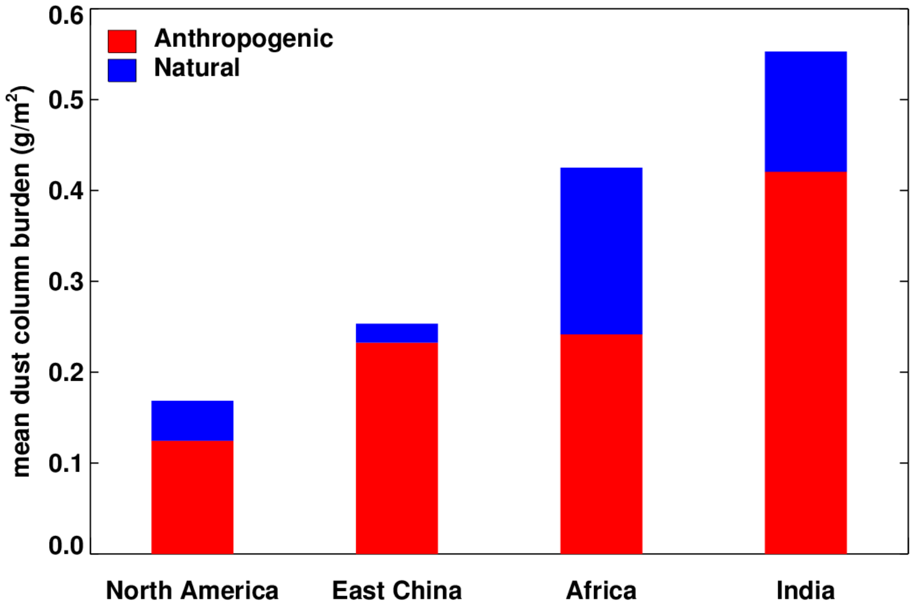


**Figure 10.** Comparison of the relative contribution of mean anthropogenic (red) and natural (blue) dust column burdens in four geographical regions.





ACPD
15, 10163–10198, 2015

Detection of anthropogenic dust using CALIPSO lidar measurements

J. Huang et al.